European Journal of Scientific Research
ISSN 1450-216X Vol.23 No.4 (2008), pp.613-625

http://www.eurojournals.com/ejsr.htm

Free Convection Boundary Layer Flow Over Cylinders of Elliptic Cross Section with Constant Surface Heat Flux

S. Ahmad
Institute for Mathematical Research, Universiti Putra Malaysia
43400 UPM Serdang, Selangor, Malaysia
E-mail: syakilaahmad@yahoo.com

N. M. Arifin
Institute for Mathematical Research, Universiti Putra Malaysia
43400 UPM Serdang, Selangor, Malaysia
E-mail: norihan@fsas.upm.edu.my

R. Nazar
School of Mathematical Sciences, Universiti Kebangsaan Malaysia
43600 UKM Bangi, Selangor, Malaysia
E-mail: rmn72my@yahoo.com
Tel: +603-89213371; Fax: +603-89254519

I. Pop
Faculty of Mathematics, University of Cluj
CP 253, R-3400 Cluj, Romania
E-mail: pop.ioan@yahoo.co.uk

Abstract

The steady laminar free convection boundary layer flow over horizontal cylinders of elliptic cross section when the major axis is both horizontal (blunt elliptic cylinder) and vertical (slender elliptic cylinder) subjected to a constant surface heat flux placed in an incompressible viscous fluid is considered in this paper. The governing boundary layer equations are solved numerically using the Keller box method. The numerical solutions are obtained for various values of the Prandtl number and parameter b/a (the ratio of the major and minor axes of the cylinder) for both blunt and slender orientations.

Keywords: Free Convection, Boundary Layer, Cylinders of Elliptic Cross Section, Constant Surface Heat Flux

1. Introduction

Free convection over a cylinder represents an important problem, which is frequently encountered in our environment and engineering services. This kind of convection occurred when the movement of the fluid is caused by density differences, which are created by the temperature differences existing in fluid mass. An example of free convection over a cylinder is the cooling process in heat exchanger components. Most of the heat exchanger components are made from tubes of non-circular cross section

such as tubes of elliptic cross section. These tubes are found to create less resistance to the cooling fluid which results in less pumping power. Therefore, the study of heat transfer from this tube is important in order to develop a compact and highly efficient heat exchanger component.

Literature on free convection boundary layer flow over a horizontal cylinder of elliptic cross section is not as extensive as for a circular cylinder (see Merkin, 1976, Ingham and Pop, 1987, Merkin and Pop, 1988, Nazar et al., 2002a, 2002b). It appears that Merkin (1977) was the first to study the free convection boundary layer on cylinders of elliptic cross section in viscous fluid, with constant surface temperature and constant surface heat flux. He solved the problem using Görtler-type expansion and Blasius series method. Bhattacharyya and Pop (1996) have solved a similar problem but only with constant surface temperature and in micropolar fluid.

In this paper, a numerical study is considered for the problem of laminar free convection boundary layer flow over horizontal cylinders of elliptic cross section when the major axis is both horizontal (blunt orientation) and vertical (slender orientation), with constant surface heat flux, immersed in a viscous fluid, using an implicit finite-difference scheme known as the Keller-box method (see Cebeci and Bradshaw, 1988). The obtained results are compared with those reported by Merkin (1977) when the Prandtl number is unity, namely Pr = 1. The numerical results are presented in figures and tables.

2. Mathematical Formulation

We consider the problem of free convection boundary layer flow over horizontal cylinders of elliptic cross section when the major axis is both horizontal and vertical, placed in a viscous and incompressible fluid of free stream velocity, U_∞ and ambient temperature, T_∞. It is assumed that the Boussinesq and boundary layer approximations are valid. Under these assumptions, the governing equations are

$$\frac{\partial \bar{u}}{\partial \bar{x}} + \frac{\partial \bar{v}}{\partial \bar{y}} = 0, \tag{1}$$

$$\bar{u}\frac{\partial \bar{u}}{\partial \bar{x}} + \bar{v}\frac{\partial \bar{u}}{\partial \bar{y}} = \upsilon \frac{\partial^2 \bar{u}}{\partial \bar{y}^2} + g\beta\left(T - T_\infty\right)\sin\phi, \tag{2}$$

$$\bar{u}\frac{\partial T}{\partial \bar{x}} + \bar{v}\frac{\partial T}{\partial \bar{y}} = \alpha \frac{\partial^2 T}{\partial \bar{y}^2}, \tag{3}$$

subject to the following boundary conditions:

$$\begin{aligned} &\bar{u} = \bar{v} = 0, \quad \frac{\partial T}{\partial \bar{y}} = -\frac{q_w}{k} \quad \text{at} \quad \bar{y} = 0, \\ &\bar{u} \to 0, \quad T \to T_\infty \quad \text{as} \quad \bar{y} \to \infty, \end{aligned} \tag{4}$$

where $\bar{x}$ is the coordinate measured along the surface of the cylinder starting from the lower stagnation point and $\bar{y}$ is the distance measured normal to it, $(\bar{u}, \bar{v})$ are the velocity components along the $(\bar{x}, \bar{y})$ axes, T is the local fluid temperature, g is the acceleration due to gravity, β is the coefficient of thermal expansion, υ is the kinematic viscosity, α is the constant thermal diffusivity of the fluid, q_w is the constant surface heat flux and k is the thermal conductivity. Further, ϕ is the angle made by the outward normal from the cylinder with the downward vertical as shown in Figure 1.

We introduce now the following non-dimensional variables:

$$\begin{aligned} &x = \bar{x}/a, \quad y = \mathrm{Gr}^{1/4}(\bar{y}/a), \quad u = \mathrm{Gr}^{-1/2}(a/\upsilon)\bar{u}, \quad v = \mathrm{Gr}^{-1/4}(a/\upsilon)\bar{v}, \\ &\theta = \mathrm{Gr}^{1/4}\left(T - T_\infty\right)/\left(aq_w/k\right), \quad \mathrm{Gr} = g\beta\left(T_w - T_\infty\right)a^3/\upsilon^2, \end{aligned} \tag{5}$$

where Gr is the Grashof number and T_w is the dimensional wall or cylinder temperature. Using (5), the basic boundary layer equations (1) to (3) can be written in non-dimensional form as

$$\frac{\partial u}{\partial x}+\frac{\partial v}{\partial y}=0, \tag{6}$$

$$u\frac{\partial u}{\partial x}+v\frac{\partial u}{\partial y}=\frac{\partial^2 u}{\partial y^2}+\theta\sin\phi, \tag{7}$$

$$u\frac{\partial \theta}{\partial x}+v\frac{\partial \theta}{\partial y}=\frac{1}{\Pr}\frac{\partial^2 \theta}{\partial y^2}, \tag{8}$$

and the boundary conditions (4) become

$$u=v=0,\quad \frac{\partial\theta}{\partial y}=-1 \quad \text{at} \quad y=0,$$
$$u\to 0,\quad \theta\to 0 \quad \text{as} \quad y\to\infty, \tag{9}$$

where Pr is the Prandtl number.

Figure 1: Physical model and coordinate system

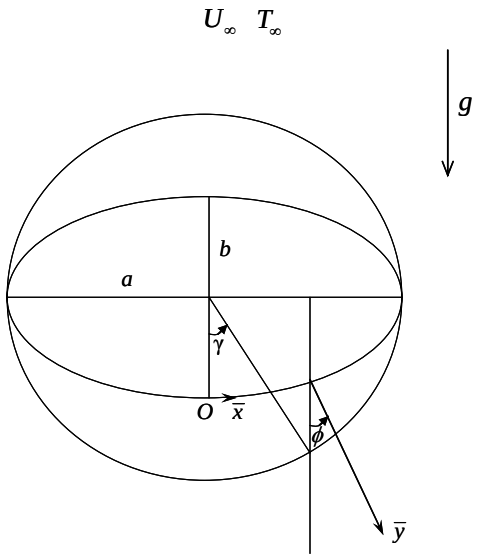

Further, we look for a solution of this system of the form

$$\psi = xf(x,y),\quad \theta=\theta(x,y), \tag{10}$$

where ψ is the stream function, which is defined as $u=\partial\psi/\partial y$ and $v=-\partial\psi/\partial x$. Substituting (10) into Eqs. (6) – (8), we get, after some algebra, the resulting equations

$$\frac{\partial^3 f}{\partial y^3}+f\frac{\partial^2 f}{\partial y^2}-\left(\frac{\partial f}{\partial y}\right)^2+\theta\frac{\sin\phi}{x}=x\left(\frac{\partial f}{\partial y}\frac{\partial^2 f}{\partial x\partial y}-\frac{\partial f}{\partial x}\frac{\partial^2 f}{\partial y^2}\right), \tag{11}$$

$$\frac{1}{\Pr}\frac{\partial^2\theta}{\partial y^2}+f\frac{\partial\theta}{\partial y}=x\left(\frac{\partial f}{\partial y}\frac{\partial\theta}{\partial x}-\frac{\partial f}{\partial x}\frac{\partial\theta}{\partial y}\right), \tag{12}$$

subject to the boundary conditions

$$f=\frac{\partial f}{\partial y}=0,\quad \frac{\partial\theta}{\partial y}=-1 \quad \text{at} \quad y=0,$$
$$\frac{\partial f}{\partial y}\to 0,\quad \theta\to 0 \quad \text{as} \quad y\to\infty. \tag{13}$$

We notice that for cylinders of circular cross section, $\sin\phi=\sin x$. However, for cylinders of elliptic cross section there are two orientations to consider, one when the major axis is horizontal and

the other when it is vertical. Following Lin and Chao (1974), these are called the blunt and slender orientations, respectively. Here x and $\sin\phi$ are given parametrically in terms of a parameter γ, as shown in Figure 1, by

$$x = \int_0^{\gamma} \left(1 - e^2 \sin^2 z\right)^{1/2} dz, \quad \sin\phi = \frac{b}{a} \frac{\sin\gamma}{\sqrt{1 - e^2 \sin^2\gamma}}, \tag{14}$$

for the blunt orientation, and

$$x = \int_0^{\gamma} \left(1 - e^2 \cos^2 z\right)^{1/2} dz, \quad \sin\phi = \frac{\sin\gamma}{\sqrt{1 - e^2 \cos^2\gamma}}, \tag{15}$$

for the slender orientation. Here b is the length of the semi-minor axis and e is the eccentricity given by $e^2 = 1 - (b/a)^2$, so that $\lambda = b/a$ is for the blunt orientation and $\lambda = (a/b)^2$ is for the slender orientation.

It can be seen that near the lower stagnation point of the cylinder, i.e. $x \approx 0$, Eqs. (11) and (12) reduce to the following ordinary differential equations:

$$f''' + ff'' + f'^2 + \lambda\theta = 0, \tag{16}$$

$$\frac{1}{\Pr}\theta'' + f\theta' = 0, \tag{17}$$

subject to the boundary conditions

$$f(0) = f'(0) = 0, \quad \theta'(0) = -1, \quad f'(\infty) = 0, \quad \theta(\infty) = 0, \tag{18}$$

where primes denote differentiation with respect to y.

In practical applications, the physical quantities of principle interest are the local skin friction coefficient and the wall or cylinder temperature, which are respectively given by

$$C_f = x\left(\frac{\partial^2 f}{\partial y^2}\right)_{y=0}, \quad \theta_w = \theta(x, 0). \tag{19}$$

3. Results and Discussion

Equations (11) and (12) subject to the boundary conditions (13) have been solved numerically using an implicit finite-difference scheme known as the Keller box method along with the Newton's linearization technique as described by Cebeci and Bradshaw (1988). The numerical solutions start at the lower stagnation point of the cylinder, $\gamma = 0$, with initial profiles as given by Eqs. (16) and (17) along with the boundary conditions (18)**Error! Reference source not found.**, and proceed round the cylinder up to $\gamma = \pi$.

Numerical results for the velocity profiles, $\partial f/\partial y$, temperature profiles, θ, as well as for the local skin friction coefficient, C_f and cylinder temperature, θ_w, have been obtained for the following values of Prandtl number: $\Pr = 0.01, 0.1, 0.7, 1, 6.8, 10$ and 100 at different positions of γ. It is worth mentioning that small values of Pr $(<<1)$ physically correspond to liquid metals, which have high thermal conductivity but low viscosity, while $\Pr \sim 1$ corresponds to diatomic gases including air. On the other hand, large values of Pr $(>>1)$ correspond to high-viscosity oils and $\Pr = 6.8$ corresponds to water at room temperature.

In order to verify the accuracy of the present method, the values of the cylinder temperature for $\Pr = 1$ with blunt and slender orientations are compared with those reported by Merkin (1977) in Tables 1,2,3 and 4. These results are found to be in good agreement. In addition, we notice that the present method allows numerical integration of Eqs. (11) and (12) to be carried out up to the top of the cylinder, given by $\gamma = \pi$, without encountering a singularity.

Numerical results for the local skin friction coefficient and cylinder temperature for various values of Pr at different positions γ or x with blunt orientation $(b/a = 0.1)$ are presented in Figures 2 and 3, respectively. It is seen from those figures that at each point of γ or x, the local skin friction coefficient and cylinder temperature increase as Pr decreases. Further, Figures 4 and 5 show the local skin friction coefficient and cylinder temperature, respectively, for various values of Pr at different positions γ or x with slender orientation $(b/a = 0.75)$. It is also seen from those figures that at each point of γ or x, the local skin friction coefficient and cylinder temperature increase as Pr decreases.

Table 1: Values of the cylinder temperature θ_w for $\Pr = 1$ with blunt orientation ($b/a = 0.1$ and 0.25) compared to Merkin (1977).

γ	***b/a*=0.1**			***b/a*=0.25**		
	x	**Present**	**Merkin (1977)**	***x***	**Present**	**Merkin (1977)**
0.0	0.0000	3.1639	3.1647	0.0000	2.6347	2.6351
0.2	0.1987	3.1549	3.1565	0.1988	2.6277	2.6287
0.4	0.3895	3.1294	3.1318	0.3901	2.6079	2.6097
0.6	0.5650	3.0869	3.0903	0.5670	2.5753	2.5780
0.8	0.7183	3.0270	3.0316	0.7231	2.5299	2.5335
1.0	0.8434	2.9494	2.9554	0.8533	2.4721	2.4767
1.2	0.9357	2.8534	2.8612	0.9544	2.4034	2.4093
1.4	0.9926	2.7407	2.7512	1.0267	2.3297	2.3365
1.6	1.0190	2.6367	2.6466	1.0796	2.2700	2.2756
1.8	1.0523	2.6067	2.6101	1.1364	2.2517	2.2543
2.0	1.1196	2.6405	2.6403	1.2167	2.2836	2.2835
2.2	1.2219	2.7404	2.7375	1.3264	2.3644	2.3621
2.4	1.3558	2.8991	2.8943	1.4646	2.4886	2.4844
2.6	1.5162	3.1071	3.1316	1.6274	2.6516	2.6455
2.8	1.6969	3.3648	3.3575	1.8092	2.8559	2.8472
3.0	1.8909	3.6995	3.6868	2.0035	3.1247	3.1107
π	2.0320	4.0463	4.0251	2.1446	3.4050	3.3829

Table 2: Values of the cylinder temperature θ_w for $\Pr = 1$ with blunt orientation ($b/a = 0.5$ and 0.75) compared to Merkin (1977).

γ	***b/a*=0.5**			***b/a*=0.75**		
	x	**Present**	**Merkin (1977)**	***x***	**Present**	**Merkin (1977)**
0.0	0.0000	2.2935	2.2943	0.0000	2.1150	2.1158
0.2	0.1990	2.2891	2.2903	0.1994	2.1135	2.1144
0.4	0.3921	2.2768	2.2784	0.3954	2.1094	2.1105
0.6	0.5739	2.2570	2.2590	0.5850	2.1034	2.1046
0.8	0.7397	2.2306	2.2331	0.7659	2.0965	2.0978
1.0	0.8866	2.1993	2.2022	0.9370	2.0904	2.0916
1.2	1.0139	2.1664	2.1694	1.0986	2.0874	2.0885
1.4	1.1244	2.1376	2.1404	1.2529	2.0904	2.0912
1.6	1.2257	2.1219	2.1238	1.4034	2.1028	2.1030
1.8	1.3286	2.1285	2.1290	1.5545	2.1278	2.1271
2.0	1.4434	2.1634	2.1623	1.7106	2.1680	2.1664
2.2	1.5763	2.2280	2.2255	1.8749	2.2255	2.2228
2.4	1.7290	2.3219	2.3180	2.0489	2.3022	2.2983
2.6	1.8999	2.4454	2.4399	2.2325	2.4015	2.3960
2.8	2.0855	2.6036	2.5959	2.4242	2.5307	2.5228
3.0	2.2809	2.8174	2.8055	2.6216	2.7102	2.6979
π	2.4221	3.0432	3.0253	2.7629	2.9041	2.8856

Table 3: Values of the cylinder temperature θ_w for $\Pr = 1$ with slender orientation ($b/a = 1$ and 0.75) compared to Merkin (1977).

γ	***b/a*=1.0**			***b/a*=0.75**		
	x	**Present**	**Merkin (1977)**	***x***	**Present**	**Merkin (1977)**
0.0	0.0	1.9966	1.9963	0.0000	1.7797	1.7808
0.2	0.2	1.9985	1.9994	0.1508	1.7866	1.7872
0.4	0.4	2.0040	2.0046	0.3059	1.8054	1.8053
0.6	0.6	2.0131	2.0135	0.4689	1.8340	1.8333
0.8	0.8	2.0260	2.0261	0.6414	1.8699	1.8687
1.0	1.0	2.0429	2.0428	0.8236	1.9106	1.9090
1.2	1.2	2.0642	2.0637	1.0143	1.9543	1.9524
1.4	1.4	2.0903	2.0894	1.2110	1.9996	1.9974
1.6	1.6	2.1220	2.1205	1.4107	2.0459	2.0432
1.8	1.8	2.1599	2.1578	1.6098	2.0928	2.0897
2.0	2.0	2.2054	2.2025	1.8051	2.1410	2.1374
2.2	2.2	2.2603	2.2562	1.9935	2.1917	2.1874
2.4	2.4	2.3272	2.3218	2.1730	2.2475	2.2423
2.6	2.6	2.4109	2.4035	2.3426	2.3131	2.3064
2.8	2.8	2.5202	2.5097	2.5030	2.3973	2.3883
3.0	3.0	2.6761	2.6597	2.6565	2.5202	2.5064
π	π	2.8491	2.8245	2.7629	2.6609	2.6407

Table 4: Values of the cylinder temperature θ_w for $\Pr = 1$ with slender orientation ($b/a = 0.5$ and 0.25) compared to Merkin (1977).

γ	***b/a*=0.5**			***b/a*=0.25**		
	x	**Present**	**Merkin (1977)**	***x***	**Present**	**Merkin (1977)**
0.0	0.0000	1.5132	1.5147	0.0000	1.1468	1.1562
0.2	0.1019	1.5315	1.5313	0.0546	1.2057	1.2096
0.4	0.2146	1.5775	1.5759	0.1308	1.3223	1.3233
0.6	0.3446	1.6402	1.6377	0.2363	1.4477	1.4469
0.8	0.4944	1.7103	1.7071	0.3705	1.5658	1.5634
1.0	0.6628	1.7818	1.7779	0.5300	1.6726	1.6687
1.2	0.8466	1.8512	1.8468	0.7094	1.7675	1.7626
1.4	1.0409	1.9169	1.9118	0.9023	1.8510	1.8455
1.6	1.2403	1.9780	1.9722	1.1015	1.9238	1.9182
1.8	1.4388	2.0342	2.0278	1.2996	1.9866	1.9815
2.0	1.6305	2.0860	2.0789	1.4893	2.0403	2.0360
2.2	1.8102	2.1343	2.1264	1.6635	2.0856	2.0823
2.4	1.9735	2.1808	2.1719	1.8161	2.1238	2.1213
2.6	2.1175	2.2292	2.2189	1.9422	2.1566	2.1584
2.8	2.2420	2.2872	2.2744	2.0389	2.1881	2.1852
3.0	2.3506	2.3736	2.3554	2.1075	2.2317	2.2237
π	2.4221	2.4804	2.4539	2.1446	2.2977	2.2771

Figures 6 and 7 show the numerical results for the local skin friction coefficient and cylinder temperature, respectively, for various values of b/a (the ratio of the major and minor axis of the cylinder) at different position γ or x with blunt orientation for $\Pr = 0.7$ (air) and 6.8 (water at room temperature). It is noticed from those figures that at each point of γ or x, the local skin friction coefficient increases and the cylinder temperature decreases as the value of b/a decreases, for both $\Pr = 0.7$ and 6.8. However, it is seen from Figures 8 and 9 that at each point of γ or x with slender orientation, the local skin friction coefficient and cylinder temperature increase as the value of b/a increases, for both $\Pr = 0.7$ and 6.8. It is also seen from Figures 6 and 8 that for each considered value of b/a, there exists a maximum value of the local skin friction coefficient, for both $\Pr = 0.7$ and 6.8 with blunt and slender orientations. It is observed from Figure 6 that for each considered value of b/a with blunt orientation, the point of γ where the local skin friction coefficient is maximum increases as the value of b/a increases, for both $\Pr = 0.7$ and 6.8. On the other hand, Figure 8 shows that for each considered value of b/a with slender orientation, the point of γ where the local skin friction coefficient is maximum decreases as the value of b/a increases, for both $\Pr = 0.7$ and 6.8.

Figures 10 and 11 display the velocity and temperature profiles at $\gamma = 0$ or $x = 0$ for various values of Pr with blunt orientation $(b/a = 0.1)$ and it is found that the velocity and temperature profiles increase as Pr decreases. It is also shown that the thermal boundary layer thickness decreases sharply with an increase in Pr. Physically, this is because, as Pr increases, the thermal diffusivity decreases. This leads to the decreasing of energy transfer ability and thus, decreases the thermal boundary layer.

Figure 2: The local skin friction coefficient for various Pr with blunt orientation $(b/a = 0.1)$.

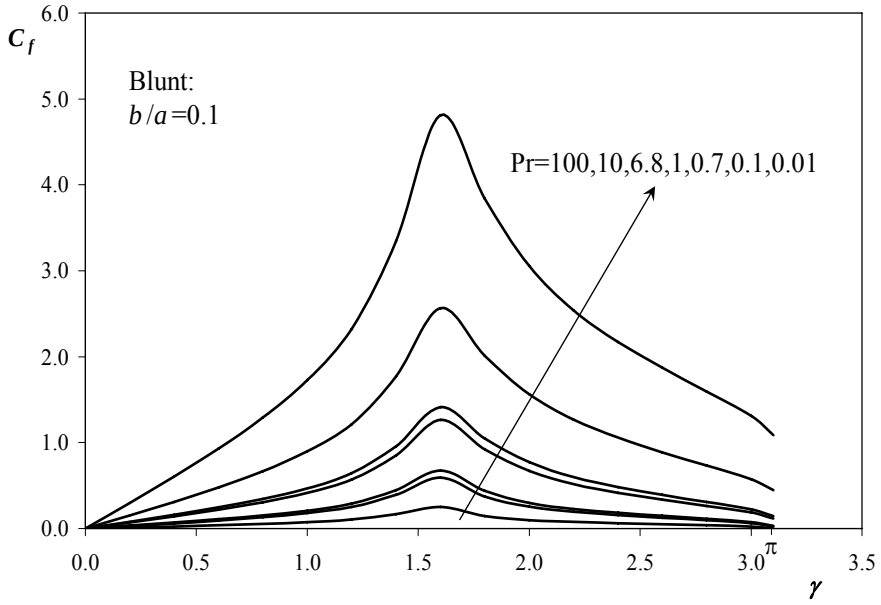

Figure 3: The cylinder temperature for various Pr with blunt orientation $(b/a = 0.1)$.

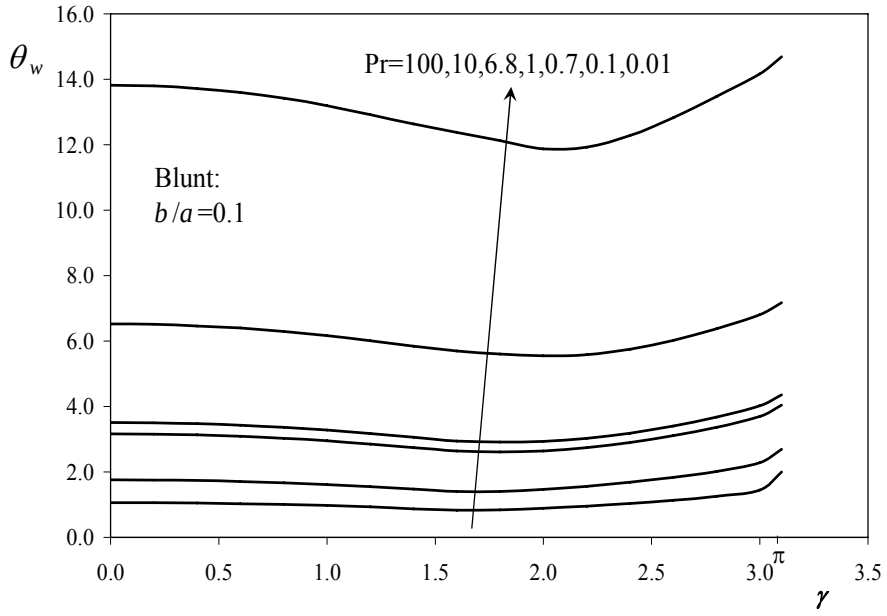

Figure 4: The local skin friction coefficient for various Pr with slender orientation $(b/a = 0.75)$.

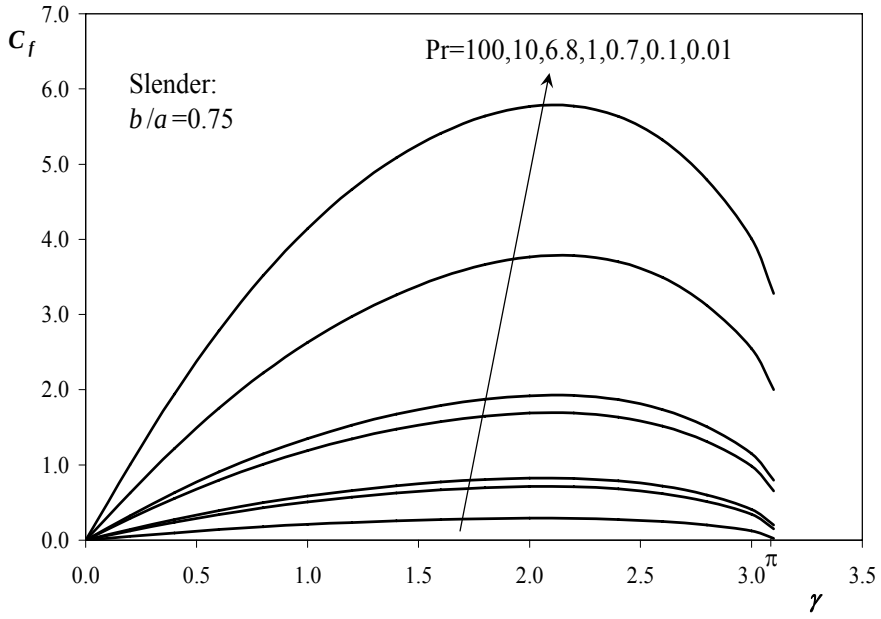

Figure 5: The cylinder temperature for various Pr with slender orientation $(b/a = 0.75)$.

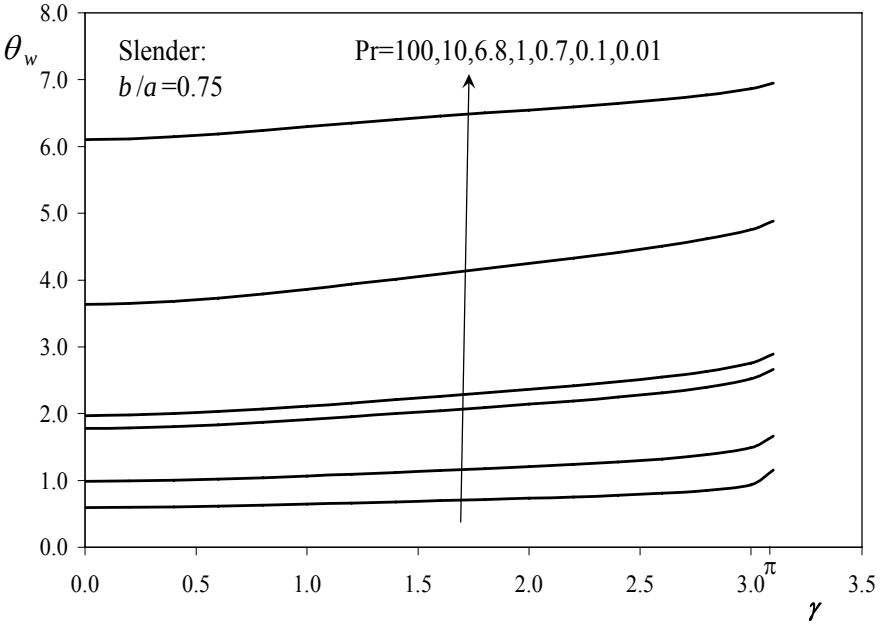

Figure 6: The local skin friction coefficient for various $\mathrm{Pr} = 0.7$ and 6.8 with blunt orientation (various b/a).

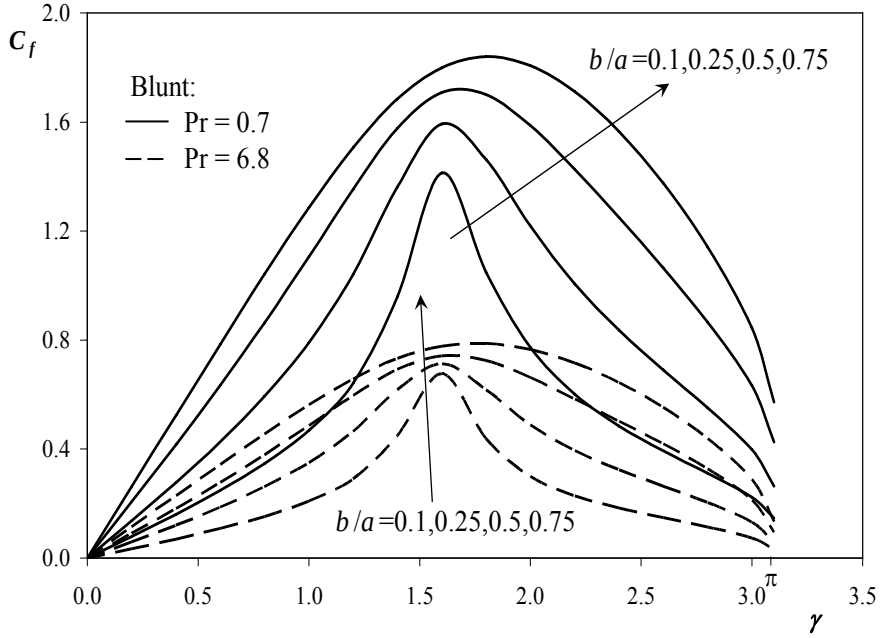

Figure 7: The cylinder temperature for $\mathrm{Pr} = 0.7$ and 6.8 with blunt orientation (various b/a).

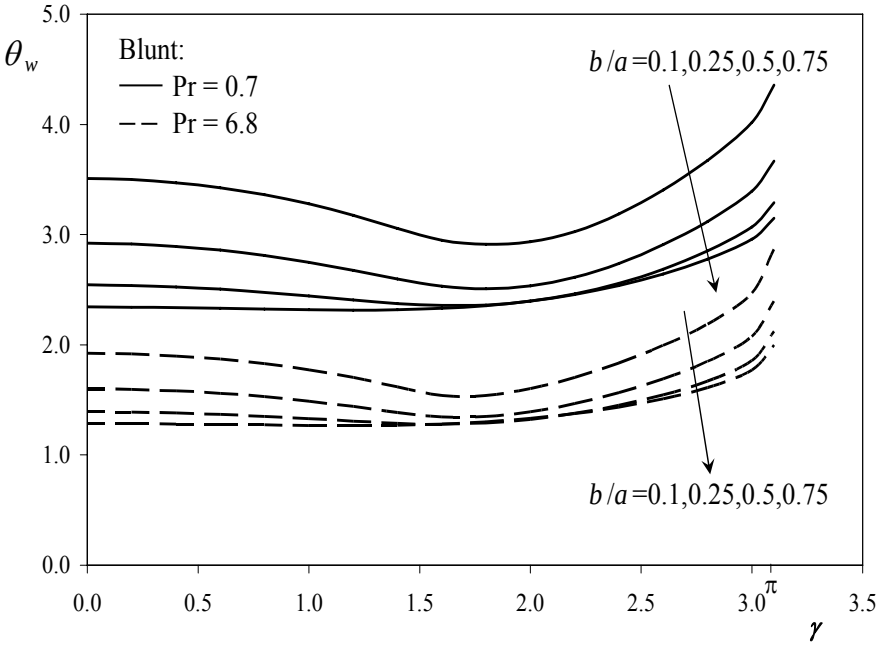

Figure 8: The local skin friction coefficient for $\Pr = 0.7$ and 6.8 with slender orientation (various b/a).

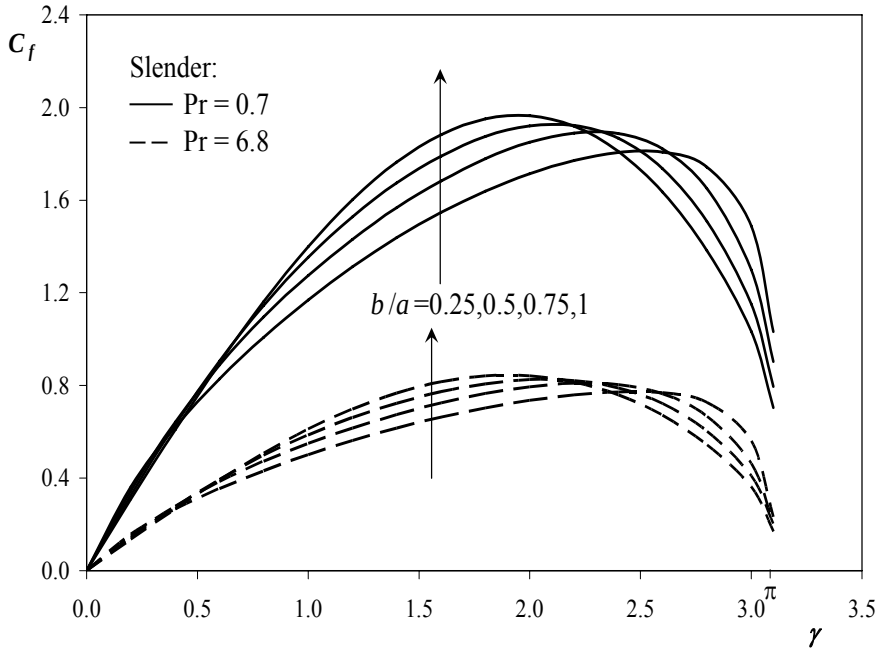

Figure 9: The cylinder temperature for $\Pr = 0.7$ and 6.8 with slender orientation (various b/a).

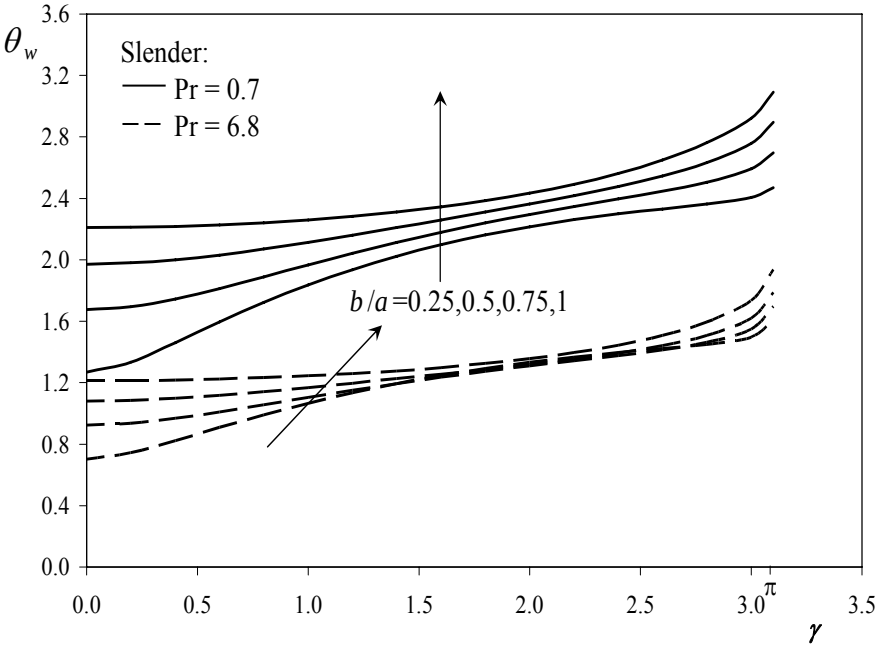

Figure 10: Velocity profiles at lower stagnation point of the cylinder, $x = 0$ for various Pr with $b/a = 0.1$ (blunt orientation).

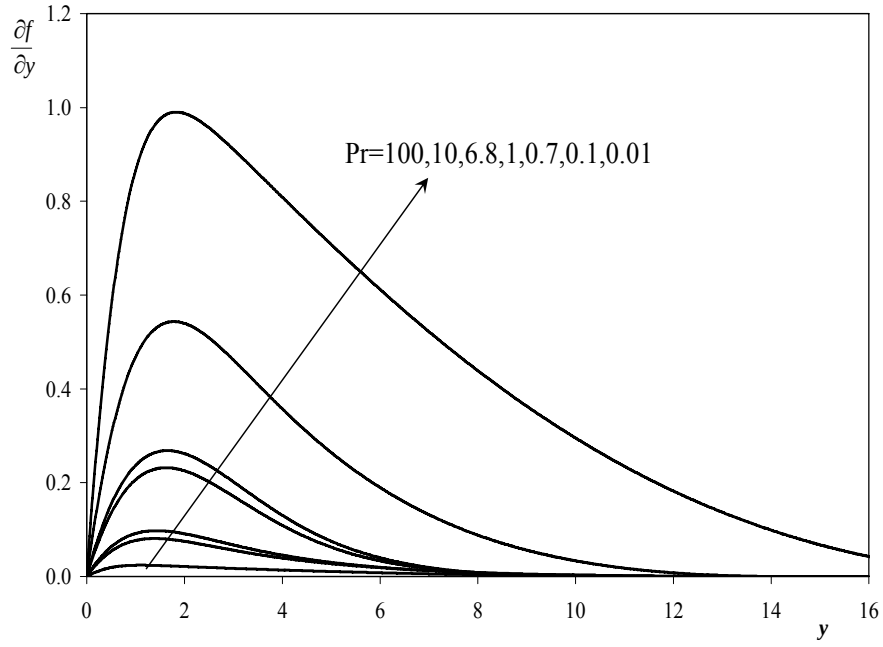

Figure 11: Temperature profiles at lower stagnation point of the cylinder, $x = 0$ for various Pr with $b/a = 0.1$ (blunt orientation).

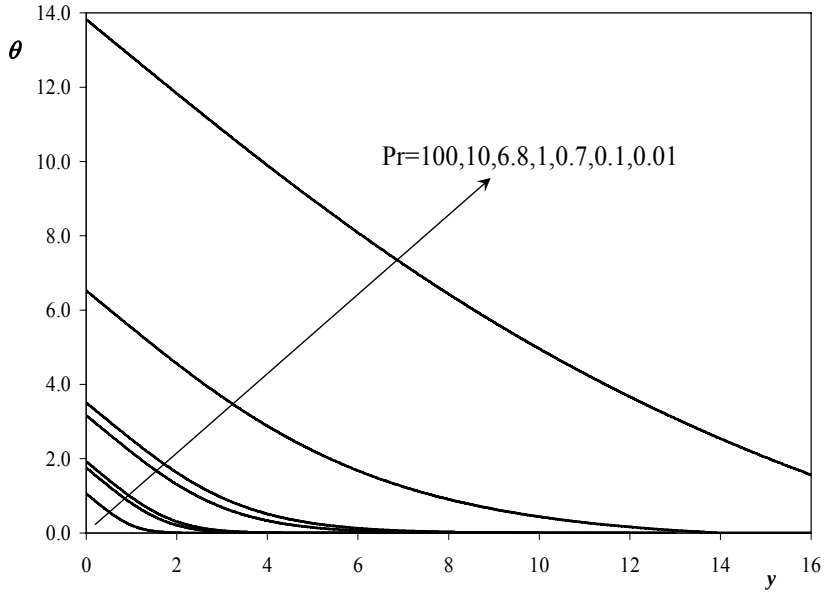

4. Conclusions

We have theoretically studied the problem of steady two-dimensional laminar free convection boundary layer flow over horizontal cylinders of elliptic cross section when the major axis is both horizontal (blunt elliptic cylinder) and vertical (slender elliptic cylinder) subjected to a constant surface heat flux and is placed in an incompressible fluid. The governing boundary layer equations were transformed using suitable transformations to a more convenient form for numerical computation. The

solutions are obtained for large and small values of the Prandtl number with various parameter b/a (the ratio of the major and minor axis of the cylinder) for both blunt and slender orientations. It is shown that the numerical values of the cylinder temperature compared well with previously published results, for some particular cases of the present problem. It is also shown from the numerical results that the velocity profiles, the temperature profiles, the local skin friction coefficient and the cylinder temperature decrease as Prandtl number increases. The results also shown that the local skin friction coefficient increases as b/a increases. However, for blunt and slender orientations, the cylinder temperature decreases and increases, respectively, as b/a increases.

Acknowledgment

The authors gratefully acknowledge the financial supports received in the form of research grants (Research University Grant Scheme (RUGS)) from the Universiti Putra Malaysia and FRGS from the Ministry of Higher Education, Malaysia.

References

[1] Bhattacharyya, S. and Pop, I., 1996. "Free Convection from Cylinders of Elliptic Cross-section in Micropolar Fluid", *International Journal of Engineering Science* 34, pp. 1301–1310.

[2] Cebeci, T. and Bradshaw, P., 1988. Physical and Computational Aspects of Convective Heat Transfer, *Springer-Verlag*, New York.

[3] Ingham, D.B. and Pop, I., 1987. "Natural Convection about a Heated Horizontal Cylinder in Porous Medium", *Journal of Fluid Mechanics* 184, pp. 157–181.

[4] Lin, F.N. and Chao, B.T., 1974. "Laminar Free Convection over Two-Dimensional and Axisymmetric Bodies of Arbitrary Contour", *Journal of Heat Transfer* 96, pp. 435–442.

[5] Merkin, J.H. and Pop, I., 1988. "A Note on the Free Convection Boundary Layer on a Horizontal Circular Cylinder with Constant Heat Flux", *Wärme und Stoffübert* 2, pp. 79–81.

[6] Merkin, J.H., 1976. Free Convection Boundary Layer on an Isothermal Horizontal Cylinder, Presented at ASME-AIChE Heat Transfer Conference.

[7] Merkin, J.H., 1977. "Free Convection Boundary Layers on Cylinders of Elliptic Cross Section", *Journal of Heat Transfer* 99, pp. 453–457.

[8] Nazar, R., Amin, N. and Pop, I., 2002a. "Free Convection Boundary Layer on a Horizontal Circular Cylinder with Constant Surface Heat Flux in a Micropolar Fluid", *International Journal of Applied Mechanics and Engineering* 7, pp. 409–431.

[9] Nazar, R., Amin, N. and Pop, I., 2002b. Free Convection Boundary Layer on an Isothermal Horizontal Circular Cylinder in a Micropolar Fluid, *Proceedings of the 12th International Heat Transfer Conference* 2, pp. 525–530.